



HAL
open science

New insights into the chemical composition and formation mechanisms of secondary organic aerosols produced in the ozonolysis of limonene

Florence JACOB, Nicolas Houzel, Paul Genevray, Cyprien Clety, Cecile Coeur, E. Perdrix, L.Y. Alleman, Sébastien Anthérieu, Guillaume Garçon, Guillaume Dhont, et al.

► To cite this version:

Florence JACOB, Nicolas Houzel, Paul Genevray, Cyprien Clety, Cecile Coeur, et al.. New insights into the chemical composition and formation mechanisms of secondary organic aerosols produced in the ozonolysis of limonene. *Journal of Aerosol Science*, 2023, 173, pp.106214. 10.1016/j.jaerosci.2023.106214 . hal-04107949

HAL Id: hal-04107949

<https://imt-nord-europe.hal.science/hal-04107949v1>

Submitted on 2 Jun 2023

HAL is a multi-disciplinary open access archive for the deposit and dissemination of scientific research documents, whether they are published or not. The documents may come from teaching and research institutions in France or abroad, or from public or private research centers.

L'archive ouverte pluridisciplinaire **HAL**, est destinée au dépôt et à la diffusion de documents scientifiques de niveau recherche, publiés ou non, émanant des établissements d'enseignement et de recherche français ou étrangers, des laboratoires publics ou privés.

1 **New insights into the chemical composition and formation mechanisms of**
2 **secondary organic aerosols produced in the ozonolysis of limonene**

3
4
5 *JACOB F.^{1,2}, HOUZEL N.^{3,*}, GENEVRAY P.⁴, CLETY C.³, COEUR C.³, PERDRIX E.¹, ALLEMAN L.Y.¹,*
6 *ANTHERIEU S.², GARCON G.², DHONT G.³, CUISSET A.³, LO GUIDICE J.-M.², TOMAS A.^{1,*}*

7
8 *¹IMT Nord Europe, Institut Mines-Télécom, Univ. Lille, Center for Energy and Environment, 59000 Lille,*
9 *France*

10 *²Univ. Lille, CHU Lille, Institut Pasteur de Lille, ULR 4483 – IMPECS – IMPact de l’Environnement*
11 *Chimique sur la Santé, F-59000 Lille, France*

12 *³Université du Littoral Côte d’Opale, UR 4493, Laboratoire de Physico-Chimie de l’Atmosphère, F-*
13 *59140, Dunkerque, France.*

14 *⁴Université du Littoral Côte d’Opale, Centre Commun de Mesures, 59140 Dunkerque, France*

15
16
17 *Corresponding authors:

18 alexandre.tomas@imt-nord-europe.fr

19 Nicolas.Houzel@univ-littoral.fr

20
21
22 Prepared for Journal of Aerosol Science

23

1 **Abstract**

2 Limonene is a wide-spread volatile organic compound in the atmosphere. Its fast reaction with ozone
3 leads to a large range of low-volatility oxygenated products that can form aerosols through gas-to-
4 particle conversion processes. However, the physical and chemical mechanisms at the origin of
5 particle formation are still fairly unknown despite the general importance of atmospheric aerosols
6 towards health and climate. In the present work, we combined experimental and theoretical
7 approaches to potentially decipher new significant mechanisms in the ozonolysis of limonene. After a
8 thorough analysis of secondary organic aerosol (SOA) chemical composition highlighting for the first
9 time the formation of oligomers up to heptamer structures as well as linear organic diacids, we
10 proposed a formation mechanism involving non-covalent hydrogen bonding implying
11 carboxylic/carbonyl/hydroxy groups. Theoretical quantum chemical calculations on dimers and
12 trimers confirmed the stability of such structures. Thus, the present results highlight the formation of
13 large oligomeric molecules whose atmospheric fate and health impacts need to be investigated.
14 More generally, it is suggested that these non-covalent H-bonds play a role in the first steps of SOA
15 formation from terpene oxidation in the atmosphere.

16

17

18

19 **Keywords**

20 Terpene, ozone, SOA, oligomers, nucleation, complexation energy

21

1 1. Introduction

2 Limonene is one of the most emitted biogenic compounds in the atmosphere with a global average
3 emission rate of 11.4 Tg per year (Guenther et al., 2012). Limonene is also largely used in home
4 deodorizers, detergents and other home products, making limonene one of the most volatile organic
5 compound (VOC) present in indoor air with concentrations that can reach hundreds of ppb during
6 cleaning events (Morawska et al., 2009; Rosales et al., 2022). The presence of two C=C electron-rich
7 double bonds in its structure confers to limonene a high reactivity. In the gas phase, the degradation
8 of limonene is principally driven by OH radicals and O₃ during the day, and by NO₃ radicals during the
9 night, with typical tropospheric lifetimes ranging from a few minutes to a few tens of minutes
10 (Atkinson & Arey, 2003; Braure et al., 2014). Regarding ozonolysis, this oxidation process is known to
11 lead to large amounts of secondary organic aerosols (SOAs) (Ahmad et al., 2017; Waring et al., 2011).
12 SOAs participate to the global burden of atmospheric aerosol, with impacts on climate change, cloud
13 formation, visibility and health (Hallquist et al., 2009; Mauderly & Chow, 2008). Noteworthy, health
14 effects of particles arising from terpene oxidation depend mainly on their size and chemical
15 composition (Rosales et al., 2022). Thus, a significant sensory irritation was observed from limonene
16 ozonolysis SOAs, although this effect could not be fully explained by the identified reaction products
17 (Baltensperger et al., 2008; Clausen et al., 2001; Rohr et al., 2002).

18 The reaction of limonene with O₃ involves ozone addition to one of the two C=C double bonds.
19 Literature reports that ozone mainly adds to the endocyclic double bond (branching ratio of about
20 90%) (Grosjean et al., 1993; Wang & Wang, 2021). Both addition reactions (to the endo- and exo-
21 cyclic double bonds) lead to a distinct primary ozonide which will decompose into excited Criegee
22 intermediates (CI). The fate of these energy-rich molecules is either a stabilization forming stabilized
23 CI (sCI) or a decomposition into an OH radical and an alkyl radical, the latter being instantaneously
24 converted into RO₂ (Johnson & Marston, 2008). Literature studies report OH radical yields of about
25 70% (Atkinson & Arey, 2003; Gong et al., 2018; Herrmann et al., 2010). The formation of low-
26 volatility products from further reactions of sCI and RO₂ leads to SOA formation (Leungsakul et al.,
27 2005).

28 In the past two decades, there have been a limited number of studies on SOA formation and
29 chemical characterization from limonene + O₃. Using on-line ion trap mass spectrometry (MS),
30 Warscheid and Hoffmann (2002) observed highly oxidised organic aerosol constituents including
31 intermediate- and low-volatility C₉ and C₁₀ polyfunctional oxygenated compounds containing
32 carbonyl and carboxyl groups (Warscheid & Hoffmann, 2002). Heaton et al. (2007) were the first to
33 detect oligomers using on-line MS and underlined the very fast formation of these compounds in
34 their reactor (Heaton et al., 2007). However, extensive fragmentation in the ionization zone of the
35 mass spectrometer precluded the identification of exact molecular masses and higher-than-dimer
36 oligomers were only suggested. The formation of oligomers was further confirmed by Walser et al.
37 (2008) and Bateman et al. (2009) who both detected more than 600 peaks in the mass-over-charge
38 (m/z) range of masses from 100 to 1000 m/z by analyzing solvent extracted SOA samples using a
39 high-resolution MS (Bateman et al., 2009; Walser et al., 2008). A mechanism involving reactions of
40 sCI with stable first-generation products was inferred to explain the formation of oligomers. Besides,
41 observing photodegradation products of SOAs produced from limonene ozonolysis, Pan et al. (2009)
42 suggested that peroxy radical reactions (RO₂+HO₂ and RO₂+RO₂) are major routes to SOA precursors
43 (Pan et al., 2009). Witkowski and Gierczak (2017) detected significant quantities of oligomers with up
44 to 20 carbon atoms in SOAs formed from the ozonolysis of limonene (Witkowski & Gierczak, 2017).
45 Contrary to Bateman et al. (2009), they advocated that esterification is an important pathway leading
46 to oligomers and SOA formation.

1

2 Because of the abundance of limonene both outdoor and indoor combined with forecasted
3 increasing background concentrations of ozone (Lin et al., 2017), it is needed to improve our
4 knowledge of the chemical composition of limonene SOAs and unravel the mechanisms yielding high
5 molecular weight oligomers. As reported above, while some SOA formation routes have been
6 suggested in the literature, large uncertainties remain regarding the exact mechanisms going from
7 gaseous products to the first SOA clusters. The objectives of the present experimental work are to go
8 deeper into the characterization of oligomers arising from the ozone reaction with limonene. A High-
9 resolution Liquid Chromatography Mass Spectrometry (LC-MS) technique was used for the analysis of
10 SOAs and theoretical calculations on oligomer structures were carried out. This allowed us to
11 propose new pathways leading to the identified oligomeric products that could be extended to other
12 terpenes.

13 **2. Experimental part**

14 Limonene ozonolysis dark reaction was operated in a laminar flow reactor described and
15 characterized elsewhere (Ahmad et al., 2017; Duncianu et al., 2012). One of the advantages of this
16 flow reactor is the possibility to maintain a constant reaction advancement over long time-periods,
17 thus enabling the sampling of large and homogeneous amounts of SOAs. The following sections
18 provide details about the generation, collection, and analysis of SOAs carried out in the present work.

19 **2.1 SOA generation**

20 The flow reactor is a tube of about 1 m length and 10 cm diameter that is separately fed by ozone
21 and limonene vapour. Ozone was produced by an O₃ generator (Air Tree Ozone Technology, C-Lasky
22 C-010-DTI or Teledyne Advanced Pollution Instrumentation O₃ calibrator Model T703) supplied by
23 pure dry zero air with a flow of 2.8-6 L/min. The ozone flow was diluted in a 100% humidified flow of
24 2.2-8 L/min of zero air and was sent to the reactor. The resulting relative humidity (RH) in the reactor
25 was about 50±5%. Pure liquid limonene (d-limonene, purity 97%, Sigma Aldrich) stored in a
26 thermostated bubbler at 293°K was flushed with a 15 mL/min flow of zero air. The vapor pressure of
27 limonene at 293°K is about 139 Pa (Clará et al., 2009) yielding a concentration of about 1370 ppm in
28 the bubbler exiting flow. This flow was rapidly diluted in a dry flow of 1 L/min of zero air and was
29 sent to the reactor. The total flow inside the tube (limonene, ozone and humid air flows) was 6-15
30 L/min, leading to a constant reaction time of 30-80 s (Duncianu et al., 2012).

31 Two contrasted experimental conditions were tested:

- 32 1. Limited oxidation conditions: a limited oxidation of limonene, where the initial ozone
33 concentration [O₃]₀ was set at a low value of 940 ppbv for an initial limonene concentration
34 of [lim]₀ = 3.1 ppmv; considering the O₃ + limonene rate constant $k = 2.01 \times 10^{-16} \text{ cm}^3$
35 $\text{molecule}^{-1} \text{ s}^{-1}$ (Shu & Atkinson, 1994) and a reaction time of 80 s, this allows to estimate that
36 about 5-10% of limonene was consumed by O₃ when leaving the reactor; three experiments
37 were done under these conditions.
- 38 2. High oxidation conditions: an advanced oxidation of limonene, where [O₃]₀ was set at a high
39 value of 50 ppmv for [lim]₀ = 1.3 ppmv; considering a reaction time of 30 s, almost 100% of
40 limonene is expected to be reacted. Two experiments were done under these conditions.

41 Thus, the properties of SOAs under weak or strong oxidative conditions could be investigated,
42 potentially reflecting fresh and aged SOAs, respectively. No OH scavenger was used in the present
43 study; therefore, both products resulting from O₃ and OH reactions with limonene (and possibly OH

1 with reaction products) are expected. No seed particles were used. The flow reactor facility was
2 hosted in an air-conditioned laboratory (295°K).

3 Ozone was monitored by a UV-absorption O₃ analyzer (O₃ 42M, Environnement SA) while limonene
4 concentrations were determined by gas chromatography coupled to dual detection by mass
5 spectrometry and flame ionization (GC-MS/FID) (Ahmad et al., 2017). Preliminary tests where ozone
6 or limonene was only present in the flow reactor indicated that stable concentrations could be
7 obtained over long time-periods (typically 8h) with a variability lower than 10%.

8 SOAs were measured by a Scanning Mobility Particle Sizer (SMPS TSI 3938L50) and a Condensation
9 Particle Counter (CPC TSI 3750). These measurements enabled to determine the size distribution and
10 the total particle number concentration (N_p), respectively. It was shown that N_p reached a maximum
11 within about 10 min after the reactant flows were set up and stayed constant over hours. The size
12 distributions displayed a monomodal (limited oxidation) or bimodal (high-oxidation) shape centered
13 around 90 nm or 60/130 nm, respectively (Figure S1). Day-to-day variability in N_p and size
14 distribution was also evaluated by comparing average N_p and sizes and it was shown that they varied
15 within 10%.

16 **2.2 SOA collection**

17 SOAs were sampled on baked quartz filters (Pallflex® Tissuquartz 2500 QAT-UP 47 mm, baked 4h at
18 500°C) at a constant flow of 5.9-8.4 L/min over 3h to 38h sampling time. A comparison of the
19 chromatograms and mass spectra obtained after the analysis of the 3h- and 38h-sampled SOA
20 showed high consistency (Figure S2), suggesting no significant impact of the sampling duration on the
21 chemical composition of the particle phase. A few filters were sampled with a home-made O₃ KI-
22 scrubber installed in front of the filter to check for potential oxidation artefacts due to O₃ interacting
23 with filter-adsorbed compounds. The filters were weighed before and after the sampling to assess
24 the sampled mass and stored in Petri boxes in a freezer at -20°C. Comparing SOA collected masses to
25 SMPS-derived masses (based on a particle density of 1.3 g/mL (Saathoff et al., 2009)) showed a good
26 agreement within 25%. Dichloromethane was used for the extraction of the filters because of its low
27 reactivity and its efficiency to solubilize organic compounds, using the following method (Bateman et
28 al., 2008): each filter was extracted twice into 5 mL of dichloromethane (≥99.5% stabilized, AnalaR
29 NORMAPUR®, VWR) followed by 30 min of sonication. The recovered volumes were then filtered
30 using syringes with 0.45 µm pore size Teflon filters before being evaporated under nitrogen flow
31 (Zymark Turbovap® LV) to 2 mL of extract per filter. The final volumes obtained were stored in glass
32 vials in the freezer at -20°C.

33 **2.3 SOA analysis: chemical composition**

34 *Elemental analysis*

35 SOAs collected on quartz filters were analysed on a Flash 2000 CHNS/O Analyser (Thermo Scientific).
36 Four punches of 8 mm diameter were taken from each sampled filter and analysed. The
37 quantification of carbon, hydrogen and oxygen contents was undertaken after calibration with
38 methionine standard (correlation coefficients >0.999). Punches from a blank filter (a baked quartz
39 filter not used) were also analysed and subtracted when necessary. Filter punches are either flash
40 burnt under oxygen (90 ml/min) at 930°C or pyrolyzed under helium (140 ml/min) at 1000°C. The
41 gases obtained are then analysed by GC/TCD (Gas chromatography coupled to Thermo Conductivity
42 Detector).

43 *LC-MS analysis*

1 The mass spectrometer used for filter extract analysis is a quadrupole - time-of-flight instrument
2 (QToF Infinity 1290 / 6540 UHD, Agilent, USA) that allows very high-resolution MS/MS analysis (Meng
3 et al., 2020). In the method applied, a volume of 5 μ L was injected on a C18 column (Agilent ZORBAX
4 Eclipse Plus C18 – 2.1 x 50 mm x 1.8 μ m) in an oven held at 40°C with a flowrate of 0.2 mL/min. The
5 mobile phase was constituted of solvent A: water with 0.1% formic acid and 5mM ammonium
6 formate, and solvent B: acetonitrile with 0.1% formic acid. The gradient was as followed: 0-2 min,
7 90% A and 10% B; 2-15 min, gradient to 50% A and 50% B; 15-20 min, gradient to 0% A and 100% B;
8 20-21 min, gradient back to 90% A and 10% B; 21-30 min, hold 90% A and 10% B. MS was performed
9 in negative and positive Electro Spray Ionisation (ESI) in scan mode from 40 to 1 700 amu. Nitrogen
10 was used as drying gas at 5 L/min and 300°C. The pressure of the nebulizer was 40 psi and the nozzle
11 voltage was 3500 V. Identification of the detected compounds was performed through MassHunter
12 Qualitative software. Molecular formulas were determined from exact masses selected in the spectra
13 and only results with mass error below 2 ppm and an identification score (calculated by the software)
14 higher than 70% were considered.

15 **2.4 Quantum chemical calculations**

16 A quantum chemical investigation of hydrogen bonding in the dimers and trimers was made with the
17 Gaussian 16 software (Frisch et al., 2019). The density functional theory (DFT) calculations were
18 performed with the B3LYP hybrid functional (Becke, 1993; Lee et al., 1988; Stephens et al., 1994;
19 Vosko et al., 1980). The correlation consistent polarized valence double-zeta atomic basis set
20 (Dunning, 1989) augmented with diffuse functions (Kendall et al., 1992) was selected to describe the
21 Kohn-Sham orbitals and the electronic density.

22 The complexation energies of dimers and trimers have been computed in order to collect evidence of
23 the possible existence of these complexes. A three-step procedure was followed. First of all, the
24 geometry of the monomers was optimized with the tight criterion of Gaussian 16 for the
25 optimization procedure. In a second stage, the optimized geometries of the monomers were used to
26 construct initial configurations for the geometry of the dimers and trimers. The relative positions of
27 the monomers in the complexes were chosen to favor intermolecular hydrogen bonds through
28 carboxylic functions. These initial guesses of geometry were then optimized, again with the tight
29 criterion. A superfine grid was selected, in order to offer a better accuracy than the default ultrafine
30 grid in the numerical integrations. The influence of the dispersion effects between the monomers
31 was taken into account by including empirical dispersion in the computation, through the D3 version
32 (Grimme et al., 2010) of Grimme's dispersion with Becke-Johnson damping (Grimme et al., 2011). We
33 confirmed that the optimizations converged to a minimum by verifying that all harmonic frequencies
34 were positive at the final geometry. In a third and last step, we performed a single point calculation
35 of the complexation energy at each of the optimized geometries. In order to minimize the effects of a
36 finite atomic orbital basis, we corrected for the basis set superposition error (BSSE) (Boys & Bernardi,
37 1970; Simon et al., 1996). The geometries of the monomers and of the complexes are available in
38 Table S1.

39 **3. Results and discussion**

40 **3.1 SOA elemental analysis**

41 The elemental composition of SOAs sampled in both limited and high oxidation conditions is given in
42 Table 1. It can be noted that this composition only slightly changes under the two oxidation
43 conditions: going from limited- to high-oxidation conditions lets the carbon and hydrogen contents
44 decrease while the oxygen part increases.

1

Table 1: Elemental analysis of SOA under limited and high oxidation conditions

	Carbon (%)	Hydrogen (%)	Oxygen (%)	O:C	H:C
Lim. oxidation SOA	56.4 (± 0.9)	8.2 (± 0.1)	34.0 (± 0.3)	0.45 (± 0.01)	1.74 (± 0.06)
High oxidation SOA	54.2 (± 2.0)	7.6 (± 0.3)	38.7 (± 0.8)	0.54 (± 0.03)	1.69 (± 0.13)

2 The O:C ratios raised from 0.45 to 0.54 when the oxidation level increases. Consistently, literature
3 reports average O:C ratios values between 0.43 and 0.50 determined from mass spectra analysis
4 under oxidative conditions of 1 - 10 ppmv for both ozone and limonene (Bateman et al., 2009; Walser
5 et al., 2008). In addition, Bateman et al. (2009) observed that the O:C value of 0.43 is quickly reached
6 after the beginning of the experiment and only slowly increases due to the further oxidation of the
7 material while at the same time H:C ratios slightly decrease from 1.585 to 1.580. While their H:C
8 ratios are lower than those found in the present work, the trend is consistent with our observations.
9 They also noticed that the O:C ratio tends to increase when the molecular weight of the reaction
10 products is higher. The present results suggest that products obtained under high-oxidation
11 conditions contain more oxygen atoms than those formed under limited-oxidation conditions.

12 The H:C ratio (1.74-1.69) only slightly decreases from limited- to high-oxidation SOAs. The H:C ratio
13 of pure limonene is 1.6 and the first ozonolysis steps (O-elimination, hydroperoxide channel and
14 ester channel) are not expected to change significantly this ratio (Johnson and Marston, 2008). Thus,
15 higher-than 1.6 H:C ratios indicate additional processes leading to an increase of the H:C ratio like the
16 condensation of oxidation products onto small molecules having high H:C ratios (formaldehyde), the
17 condensation of water onto particles or the loss of CO₂ during the decomposition of carbonyl oxides
18 (Walser et al., 2008). Bateman et al. (2009) noted no significant change in the H:C ratios (from about
19 1.58 to 1.60) with increasing relative humidity from dry to 40% (Bateman et al., 2009). Consistently,
20 the hygroscopicity of SOA from monoterpene ozonolysis is known to be limited, with a growth factor
21 of about 1.065 at 85% relative humidity (Varutbangkul et al., 2006). Therefore, the condensation of
22 H₂O through hydration reactions may have a limited impact on the chemical composition of SOAs.

23

24 Oxygen-to-carbon ratios determined on ambient aerosol in various places across Europe display
25 values around 0.41 for semi-volatile oxygenated organic aerosol and 0.89 for low-volatile, more
26 oxidized oxygenated organic aerosol (Crippa et al., 2014; Poulain et al., 2021). Consistently,
27 hydrogen-to-carbon ratios around 1.70 have been found to characterize semi-volatile oxygenated
28 organic aerosol (Poulain et al., 2021). While the present limonene and ozone concentrations are
29 more representative of indoor environments, the calculated ratios reported in Table 1 show rather
30 low oxygenated SOA.

31 **3.2 SOA LC-MS analysis**

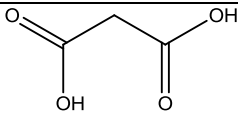
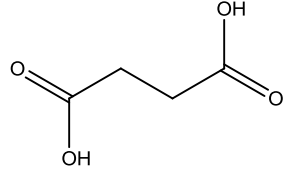
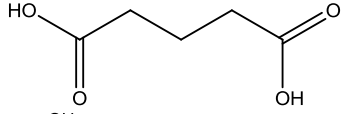
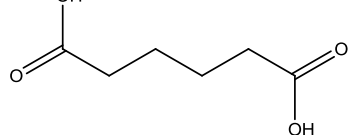
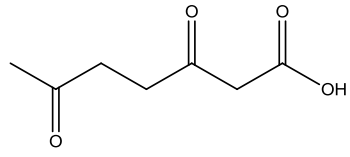
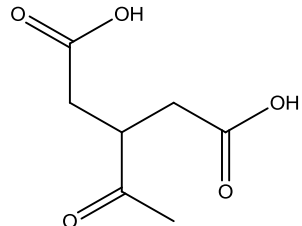
32 LC-MS analyses were performed to determine the chemical composition of SOA obtained under the
33 two different operating conditions. As mentioned in the section 2.2, one sample was also collected
34 with an O₃ scrubber in front of the filter (limited limonene oxidation). The results of this sample are
35 similar to the sample without scrubber and will not be discussed specifically. This indicates that on-
36 filter oxidation by ozone is probably not significant in the present experimental conditions.

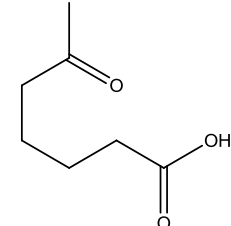
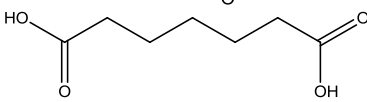
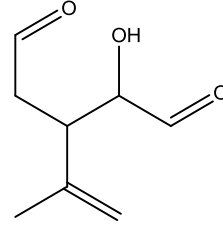
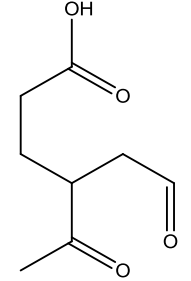
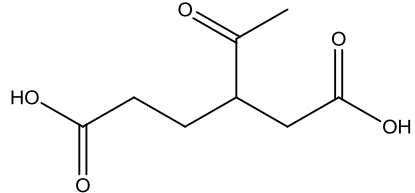
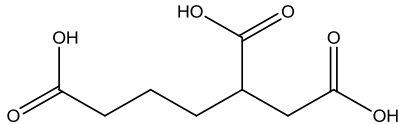
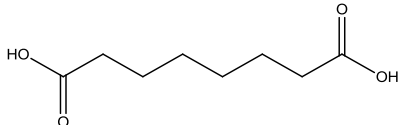
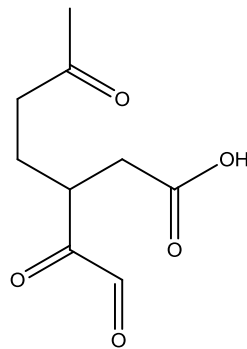
37 Examples of total ion chromatograms (TIC) resulting from the LC-MS analyses are shown in Figure S3
38 in the Supplementary Material. They exhibit a few well-defined chromatographic peaks together with
39 very large peaks underlining the presence of a multitude of co-eluting compounds. TIC from limited-
40 and high-oxidation present strong similarities. We will thus present the common features in the
41 following sections before highlighting the differences.

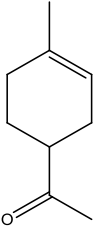
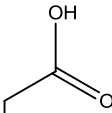
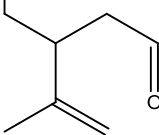
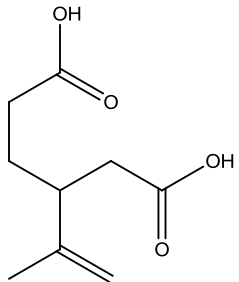
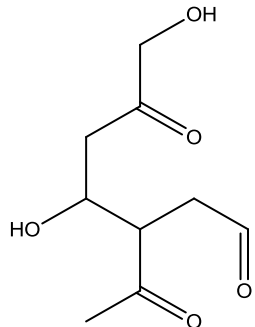
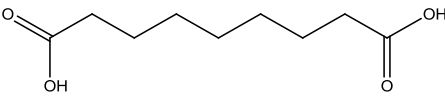
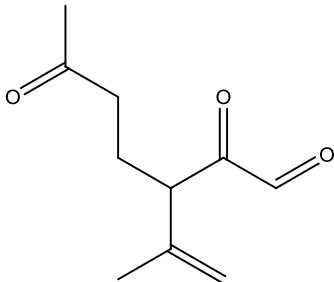
1 *First- and second-generation products*

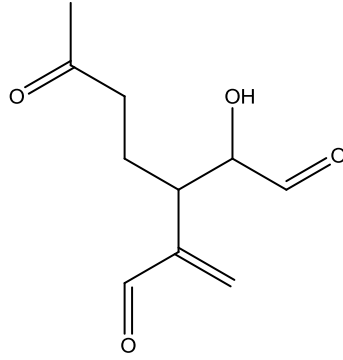
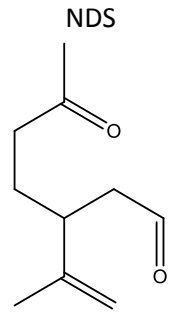
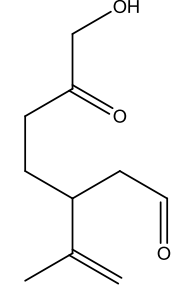
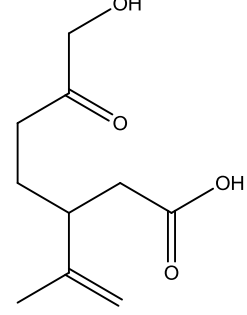
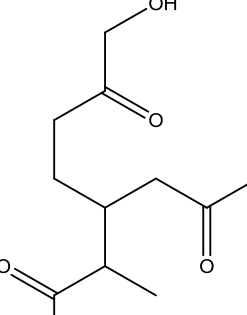

2 First- and second-generation products of limonene + O₃ already identified in the literature (Bateman
 3 et al., 2009; Gong et al., 2018; Hammes et al., 2019; Kundu et al., 2012; Leungsakul et al., 2005;
 4 Walser et al., 2008; Warscheid & Hoffmann, 2002) were looked for in the chromatograms. The
 5 presence of all the raw formulas listed in Table 2 was confirmed through their detection in the
 6 positive ((M+H)⁺ or (M+NH₄)⁺ adducts) or negative ionization modes ((M-H)⁻ adducts) depending on
 7 the proton affinity of the extracted compound. Overall, 34 raw chemical formulas were identified
 8 with high confidence and possible structures are proposed, mostly based on literature findings (Table
 9 2). Most of these compounds contain hydroxyl, carbonyl and/or carboxylic acid functions. Hammes
 10 et al. (2019) underlined that large amounts of organic acids were observed particularly in the particle
 11 phase (Hammes et al., 2019). Extracted ion chromatograms (EIC) were then obtained based on the
 12 ion masses corresponding to the 34 raw formulas. Interestingly, while a few EIC display one single
 13 peak, the majority shows either many peaks or large peaks (Figure S4) similar to the TIC over the
 14 whole chromatogram.

15 **Table 2:** Summary of the monomers detected in limonene+O₃ SOA (raw formula and tentative
 16 structures based on the references quoted)
 17

Raw formula	MW	Ionization	m/z	Score	Structures*
C ₃ H ₄ O ₄	104	(M-H) ⁻	103.0037	99.76	
C ₄ H ₆ O ₄	118	(M-H) ⁻	117.0193	99.99	
C ₅ H ₈ O ₄	132	(M-H) ⁻	131.0350	99.96	
C ₆ H ₁₀ O ₄	146	(M-H) ⁻	145.0506	99.9	
C ₇ H ₁₀ O ₄ ^a	158	(M-H) ⁻	157.0506	99.69	
C ₇ H ₁₀ O ₅ ^a	174	(M-H) ⁻	173.0455	100	

$C_7H_{12}O_3^a$	144	(M-H) ⁻	143.0714	100	
$C_7H_{12}O_4$	160	(M-H) ⁻	159.0663	99.81	
$C_8H_{12}O_3$	156	(M-H) ⁻	155.0714	99.99	
$C_8H_{12}O_4^{a,b}$	172	(M-H) ⁻	171.0663	99.74	
$C_8H_{12}O_5^a$	188	(M-H) ⁻	187.0612	99.18	
$C_8H_{12}O_6$	204	(M-H) ⁻	203.0561	100	
$C_8H_{14}O_3^a$	158	(M+H) ⁺ (M+NH ₄) ⁺ (M+H) ⁺	159.1012 176.1278 175.0962	99.22 99.42 99.56	NDS
$C_8H_{14}O_4$	174	(M+NH ₄) ⁺	192.1229	99.9	
$C_9H_{12}O_4^a$	184	(M-H) ⁻	183.0663	99.25	NDS
$C_9H_{12}O_5^a$	200	(M-H) ⁻	199.0612	100	
$C_9H_{12}O_6^a$	216	(M-H) ⁻	215.0561	99.62	NDS

$C_9H_{14}O^c$	138	$(M-H)^-$	137.0972	99.07	
$C_9H_{14}O_2$	154	$(M-H)^-$	153.0921	99.47	NSD 
$C_9H_{14}O_3^{b,d,e}$	170	$(M-H)^-$	169.087	100	
$C_9H_{14}O_4^{a,b,c,d,e}$	186	$(M-H)^-$	185.0819	99.99	
$C_9H_{14}O_5^{a,b,e}$	202	$(M-H)^-$	201.0768	99.9	
$C_9H_{16}O_3$	172	$(M+H)^+$	173.1173	99.97	NDS 
$C_9H_{16}O_4$	188	$(M+H)^+$	189.1119	99.72	
		$(M+NH_4)^+$	206.1385	99.83	
$C_{10}H_{14}O_3^{c,d}$	182	$(M-H)^-$	181.087	99.96	

$C_{10}H_{14}O_4^d$	198	$(M-H)^-$	197.0819	99.98	
$C_{10}H_{14}O_5^a$	214	$(M-H)^-$ $(M+H)^+$	213.0768 169.1221	99.99 99.77	NDS 
$C_{10}H_{16}O_2^{b,c,d}$	168	$(M+NH_4)^+$	186.1487	99.87	
$C_{10}H_{16}O_3^{a,b,c,d,e}$	184	$(M-H)^-$	183.1027	99.99	
$C_{10}H_{16}O_4^{a,b,d}$	200	$(M-H)^-$	199.0976	99.84	
$C_{10}H_{16}O_5^f$	216	$(M-H)^-$	215.0925	99.82	

$C_{10}H_{16}O_6^f$	232	(M-H) ⁻	231.0874	99.8	
$C_{10}H_{18}O_4$	202	(M+NH ₄) ⁺	220.1541	99.73	

1 *a: (Hammes et al., 2019); b: (Walser et al., 2008); c: (Leungsakul et al., 2005); d: (Bateman et al., 2009); e:*
2 *(Kundu et al., 2012); f: (Warscheid & Hoffmann, 2002).*

3 ** One structure shown as example, but different structures could fit a same raw formula.*

4 *NDS: No Defined Structure*

5

6 *Oligomer identification*

7 The mass spectra recorded over the LC-MS chromatograms show clear evidence for the presence of
8 large oligomer structures. Figure 1 presents a typical mass spectrum (at a retention time of 11.1 min)
9 displaying such oligomer formations with up to seven regular modes corresponding to monomer
10 (~45-250 m/z), dimer (~290-490 m/z), trimer (~490-680 m/z), tetramer (~680-880 m/z), pentamer
11 (~880-1050 m/z), hexamer (~1050-1300 m/z), until heptamer (~1300-1500 m/z) compounds.
12 Oligomers were already observed in the ozonolysis of VOCs using offline and online techniques (laser
13 desorption ionization and electrospray ionization mass spectrometry, ion cyclotron resonance
14 Fourier transform mass spectrometry), both in controlled lab-experiments and in the atmosphere
15 (Baltensperger et al., 2005; Kalberer et al., 2004; Kourtchev et al., 2016; Ofner et al., 2011; Tolocka et
16 al., 2004; Yang et al., 2020). However, the present work shows, for the first time, oligomeric
17 structures up to heptamers in the ozonolysis of monoterpenes.

18 An interesting point regarding the mass transitions between one oligomer area to the next one
19 (inter-mode transitions), is that they systematically correspond to the exact masses of first- and
20 second-generation products of limonene ozonolysis (Figure 1, Table 3 and Table S2).

21

22 **Table 3:** Oligomers M₁ and M₂ identified and highlighted in Figure 1 and the monomer
23 responsible for the transition between oligomers M₁ and M₂.

Identified monomer/oligomer M ₁			Identified monomer/oligomer M ₂			Monomer responsible for the transition M ₁ → M ₂		
(M ₁ -H) ⁻	M ₁ brut formula	Score	(M ₂ -H) ⁻	M ₂ brut formula	Score	Transition (M ₂ -H) ⁻ - (M ₁ -H) ⁻	Transition brut formula	Score
197.0820	$C_{10}H_{14}O_4$ (monomer)	99.98	369.1559	$C_{18}H_{26}O_8$ (Dimer)	99.52	172.0739	$C_8H_{12}O_4$ (Monomer)	99.37
			369.1913	$C_{19}H_{30}O_7$ (Dimer)	99.05	172.1093	$C_9H_{16}O_3$ (Monomer)	97.8

415.1971	C ₂₀ H ₃₂ O ₉ (Dimer)	99.83				186.0868	C ₉ H ₁₄ O ₄ (Monomer)	77.82
399.1660	C ₁₉ H ₂₈ O ₉ (Dimer)	99.9	601.2839	C ₂₉ H ₄₆ O ₁₃ (Trimer)	89.61	202.1179	C ₁₀ H ₁₈ O ₄ (Monomer)	76.17
431.1930	C ₂₀ H ₃₂ O ₁₀ (Dimer)	98.72				170.0909	C ₉ H ₁₄ O ₃ (Monomer)	<70
601.2839	C ₂₉ H ₄₆ O ₁₃ (Trimer)	89.61				787.3734	C ₃₈ H ₆₀ O ₁₇ (Tetramer)	93.61
787.3734	C ₃₈ H ₆₀ O ₁₇ (Tetramer)	93.61	973.4605	C ₄₇ H ₇₄ O ₂₁ (Pentamer)	85.56	186.0871	C ₉ H ₁₄ O ₄ (Monomer)	81.83
973.4605	C ₄₇ H ₇₄ O ₂₁ (Pentamer)	85.56	1159.5502	C ₅₆ H ₈₈ O ₂₅ (Hexamer)	90.57	186.0897	C ₉ H ₁₄ O ₄ (Monomer)	98.78
1159.5502	C ₅₆ H ₈₈ O ₂₅ (Hexamer)	90.57	1345.6373	C ₆₅ H ₁₀₂ O ₂₉ (Heptamer)	84.02	186.0871	C ₉ H ₁₄ O ₄ (Monomer)	81.23

1

2 Thanks to the mass precision of the ToF-MS (< 2 ppm), it is possible to precisely identify the raw
3 formula of the species involved in the transitions from one group of oligomers to another one (called
4 inter-mode transitions in the following). In addition, transitions within an oligomer area (called intra-
5 mode transitions, Figure 2) are mainly characterized by mass differences of m/z 14 and 16. The
6 regularity of the mass transitions was already underlined in previous laboratory studies on other
7 chemical systems (Baltensperger et al., 2005; Kalberer et al., 2004; Tolocka et al., 2004) and field
8 campaigns (Yang et al., 2020). More rarely, transitions of m/z = 10, 12 or 18 are observed in the
9 present work. MS identification of the raw chemical formulas shows that these transitions are linked
10 to a gain or a loss of CH₂ (transitions m/z = 14) and O (transitions m/z = 16) on the oligomer chain
11 (Figure 2 and Table 4). It should be stressed that most of the limonene ozonolysis products have a
12 difference of a multiple of CH₂ (ex: C₁₀H₁₆O₄/C₉H₁₄O₄) or O₂ (ex: C₁₀H₁₆O₃/C₁₀H₁₆O₄) and scarcely a
13 difference of m/z = 10 (ex: C₈H₁₄O₄/C₉H₁₂O₄), 12 (ex: C₈H₁₂O₄/C₁₀H₁₆O₃) or 18 (ex: C₁₀H₁₆O₃/C₉H₁₄O₅).
14 The difference of mass 18 could be due to water loss in aldol condensation or esterification reactions
15 (Bateman et al., 2009) or water addition through hydration reactions, as suggested in the section 3.1
16 "SOA elemental analysis". Thus, these regular intra-mode mass transitions reveal that oligomer
17 chains are composed of molecules matching first- and second-generation products and sCI, the
18 chains growing either through addition of monomers without any atom/fragment loss or through
19 reactions between sCI and monomers or higher oligomers.

20 **Table 4:** Identification of the oligomers M₁ and M₂ linked by a difference of m/z = 14 (CH₂) and 16 (O)
21 as displayed in Figure 2.

(M ₁ -H) ⁻	M ₁ brut formula	Score	(M ₂ -H) ⁻	M ₂ brut formula	Score	Transition M ₂ -M ₁
541.2662	C ₂₇ H ₄₂ O ₁₁	98.92	555.2798	C ₂₈ H ₄₄ O ₁₁	97.08	CH ₂
555.2798	C ₂₈ H ₄₄ O ₁₁	97.08	571.2746	C ₂₈ H ₄₄ O ₁₂	96.67	O
571.2746	C ₂₈ H ₄₄ O ₁₂	96.67	585.2899	C ₂₉ H ₄₆ O ₁₂	95.05	CH ₂
585.2899	C ₂₉ H ₄₆ O ₁₂	95.05	601.2839	C ₂₉ H ₄₆ O ₁₃	89.61	O
601.2839	C ₂₉ H ₄₆ O ₁₃	89.61	617.2826	C ₂₉ H ₄₆ O ₁₄	98.04	O
617.2826	C ₂₉ H ₄₆ O ₁₄	98.04	631.2970	C ₃₀ H ₄₆ O ₁₄	99.97	CH ₂

22

23 *Oligomer formation processes*

1 Although a few hypotheses were made regarding the formation mechanisms of these oligomers
2 (accretion of RO₂ radicals, esterification, reactions involving sCl), the exact mechanisms still remain
3 unknown. It is worth noting that oligomerization processes such as RO₂ accretion (RO₂ + RO₂ → ROOR
4 + O₂, (Jokinen et al., 2014; Pan et al., 2009)) or esterification (alcohol + acid → ester + H₂O, (Bateman
5 et al., 2009)) proceed through losses of atoms/fragments; therefore, regarding the intra-mode
6 observed in this study, they might not fully explain oligomer formation. Regarding organic peroxide
7 formation through RO₂ accretion reactions, while this mechanism cannot be ruled out, the fairly high
8 lability of organic peroxides may hamper them to remain in the collected SOA samples (Krapf et al.,
9 2016). Clustering of small oligomers in the ESI source of the MS could also be neglected, since the
10 analysis of samples diluted from 100 to 1000 times did not show any difference in the global shape of
11 the chromatograms, with a steady elution of oligomers with different masses supposed to arise from
12 a partial oligomer degradation in the ionization source leading to smaller-size oligomers. Note also
13 that Gao et al. tested individual monomers and cocktails of monomers with an ESI source and
14 concluded that only minimal amounts of dimers could be observed, thus precluding any significant
15 impact of the ESI source on oligomer formation (Gao et al., 2004).

16 A few literature studies suggest that the ozonolysis of unsaturated VOCs like monoterpenes can be
17 followed by dimerization and trimerization through non-covalent hydrogen bonds involving
18 carboxylic functional groups, dicarboxylic functional groups and near ketones/alcohol functional
19 groups (Claeys et al., 2009; Hoffmann et al., 1998; Figure S5). First- and second-generation products
20 identified in the present work possess such functional groups (Table 2) enabling them to form this
21 type of non-covalent bonds. Intramolecular H-bonds in complex oxygenated molecules are expected
22 to hamper the formation of clusters. Yet, the detection of all the monomers in the oligomer elution
23 region with exactly the mass of the first- and second-generation products strongly suggests their
24 participation in the formation of the oligomers and limited intramolecular bonds. The oligomers
25 observed in this work in the limonene ozonolysis SOAs support processes involving intermolecular
26 hydrogen bonding between first- and second-generation products.

27 Moreover, the presence of non-covalent hydrogen bonds is supported by comparing chromatograms
28 issued from monomer and oligomer ion extractions. For example, the EIC for the C₉H₁₄O₄ monomer
29 and their corresponding homodimer C₁₈H₂₈O₈ and homotrimer C₂₇H₄₂O₁₂ are superposed in Figure 3.
30 On the monomer signal, four major peaks are observed: a first one elutes at 1.1 min corresponding
31 to one monomeric compound with C₉H₁₄O₄ formula; a second peak is also detected at 1.6 min and
32 two others at 3.4 and 3.6 min. The homodimer extracted chromatogram exhibits one major peak at
33 1.6 min: the presence of a signal for the monomer and homodimer at a strictly identical retention
34 time (1.6 min) suggests that the homodimer is partly decomposed in its monomer during the analysis
35 in the ionization source of the MS. The peaks at 3.4 and 3.6 min might be due to two isomers of the
36 monomeric compound eluting at 1.1 min. Regarding the homotrimer chromatogram, no
37 chromatographic peak can be observed but only a tiny baseline increase between 5.0 and 6.5 min.
38 This suggests that the homotrimer C₂₇H₄₂O₁₂ is probably in negligible amount in the SOA sample.
39 Similar overlapped chromatographic profiles were observed for other monomers such as C₈H₁₂O₄,
40 C₉H₁₄O₃, C₉H₁₄O₄, C₉H₁₄O₅, C₁₀H₁₆O₃ and C₁₀H₁₆O₄.

41 In addition, in a previous article published by our group (Meng et al., 2020) analyzing the SOAs
42 formed from the reaction between guaiacol and NO₃ using the same LC-MS setup, it is reported that
43 the aerosols are composed of a mixture of nitroguaiacol and dimers of nitroguaiacol linked by
44 covalent peroxide bonds. Contrary to the present work, no decomposition was noted for the dimeric
45 compounds (Figure S6) although the peroxide bond is known to be fairly weak (Bach et al., 1996).
46 Therefore, the observed decomposition of homodimers in the soft ESI source suggests that the bond

1 energy between the two monomers is lower than a typical covalent bond. This will be discussed later
2 on in section 3.3.

3 Apart from the non-covalent H-bond association reactions suggested above, other pathways like
4 esterification, aldolisation and sCl reactions cannot be excluded among the processes leading to
5 oligomers (Bateman et al., 2009; Kalberer et al., 2004; Tolocka et al., 2004; Witkowski & Gierczak,
6 2017; Yasmeen et al., 2010). For example, the structural isomers with raw formula $C_{18}H_{28}O_6$ identified
7 in the present work is suggested to be formed by esterification or aldolisation (Witkowski & Gierczak,
8 2017). The EIC of the corresponding mass shows 4 main chromatographic peaks followed by an
9 increase of the signal in the oligomer elution area (Figure S7), indicating that the $C_{18}H_{28}O_6$ isomers
10 are present in the condensed phase both as single compounds (under different isomer forms, Figure
11 S8) and also participating in many oligomer structures (Figure S9). The same behaviour has been
12 noted for compounds such as $C_{19}H_{28}O_7$ and $C_{19}H_{30}O_5$.

13 A distinction has to be made between the two main types of components of the SOAs studied: the
14 single compounds and the oligomers. Single compounds, including monomers and dimers with
15 covalent or non-covalent bonds, exhibit separate chromatographic peaks on their EIC (Figure S4).
16 These well-defined peaks are often followed by an increased baseline signal in the oligomer area
17 eluting from ~3.0 to 20.0 min. The significant contribution of monomer and dimer signals in the
18 oligomer area indicates that they participate in oligomeric compounds, which partly decompose
19 either during elution or, more probably, in the ionization source of the MS giving rise to a
20 monomeric/dimeric signal. Furthermore, the instability of oligomers during the elution and/or the
21 ionization process stresses the relative fragility of the bonds between each monomer and supports
22 the hypothesis of non-covalent bonds (see also the theoretical calculations below). The poor
23 chromatographic separation observed for oligomers in the analytical conditions of this study is
24 consistent with the observation of oligomers nearly over the whole chromatograms. Their
25 concentration and size raise along the chromatogram to reach heptamers and maximum
26 concentrations between 10-12 min. Noteworthy, literature studies reported the use of LC-MS
27 techniques to identify H-bonding clusters (Claeys et al., 2009; Hoffmann et al., 1998; Yasmeen et al.,
28 2010).

29 *Diacidic compounds*

30 Interestingly, C3 to C10 linear diacids were also identified for the first time in limonene ozonolysis
31 products (Table 2). Note that C4-C6 diacids were observed in limonene photo-oxidation chemistry
32 (Jaoui et al., 2006). Their unexplained presence was attributed to heterogeneous/multiphase
33 processes. The corresponding EIC (Figures 4a and S10a-c) display a limited number of peaks and an
34 almost flat signal in the oligomer area for the short linear diacids. For the C6 (adipic), C7 (pimelic),
35 and C8 (suberic) diacids, the signal in the oligomer elution area slightly increases with the raise of the
36 diacid size (Figures 5b and S10d), indicating that these diacids may participate in oligomer structures.
37 Indeed, some diacids were shown to favour intramolecular hydrogen bonds (Claeys et al., 2009). In
38 the case of linear diacids, the distance between two acid functions may play a role for non-covalent
39 bonds with short distance favouring intramolecular hydrogen bonds and long distance favouring
40 intermolecular hydrogen bonds (Figure S5).

41 Literature reports the formation of dimers and cyclic trimers through H-bonding of compounds
42 containing one carboxylic functional group (Csanko, 2015). Although limonene SOA products with a
43 single carboxylic function (like 6-oxo-pentanoic acid, Table 2) may similarly participate to the
44 formation of dimers and cyclic trimers, there is no evidence yet in the literature about the formation
45 of cyclic tetramers or larger cyclic oligomers from such monoacid molecules. However, the

1 participation of diacid compounds in the formation of higher oligomers may be envisioned in
2 facilitating the connection of monomers and dimers through non-covalent H-bonds (Figure S11).

3 *Differences between the limited and high oxidation samples*

4 While oligomer formation is clear in both limited- and high-oxidation samples, as expected the latter
5 seems to present oligomers with higher masses. A limited oxidation of limonene by ozone restrains
6 the formation of higher-generation products, whereas under strong oxidation the two limonene
7 double bonds will react with ozone leading to more oxidized and heavier monomeric and oligomeric
8 compounds. This observation is also supported by the disappearance of unsaturated compounds in
9 the high oxidation sample as the $C_{10}H_{16}O_3$ monomer (see Figure S12) and the three dimers $C_{18}H_{28}O_6$,
10 $C_{19}H_{28}O_7$ and $C_{19}H_{30}O_5$ (not shown).

11 **3.3 Theoretical calculations**

12 *Monomers*

13 We considered two molecules for the calculations, one with a carboxylic acid function, the limonic
14 acid ($C_9H_{14}O_3$) and one with both ketone/alcohol functions, the 7OH-limonaldehyde ($C_{10}H_{16}O_3$). These
15 two molecules have been chosen due to their similar structures to investigate the possibilities of
16 dimerization and trimerization by non-covalent hydrogen bonds of functions present in the products
17 observed in SOAs formed from limonene ozonolysis.

18 The two structures have been built as stabilized geometries with potential intramolecular hydrogen
19 bonds and then optimized by Gaussian in order to find the minimum of the potential energy surface
20 close to these initial geometries (Figure S13).

21 *Complexation energy of dimers and homotrimers*

22 Dimers with intermolecular hydrogen bonds are well known in literature to form stable structures
23 (even more stable than lone monomer like acetic acid homodimer in the gas phase at room
24 temperature (Goubet et al., 2015)). In our calculations, the monomer initial positions were chosen to
25 favour intermolecular hydrogen bonds through carboxylic functions. The values of the complexation
26 energies are given in Table 5. The raw values were computed without BSSE correction, while the
27 corrected values take care of the BSSE. Typically, it is expected that the raw values are larger in
28 absolute value than the corrected ones, because one monomer of a complex can artificially lower its
29 energy using the atomic basis set of the other monomers of the complex (Kestner & Combariza,
30 1999). This statement is verified in Table 5, which suggests that all the five considered complexes
31 should be formed in the experiments presented in the paper. Carboxylic acid homodimers are more
32 stable than ketone/alcohol homodimers, but both are possible and are more stable than the two
33 separate molecules. As expected, the intermolecular hydrogen bonds for cyclic dimers happen
34 through carboxylic functions (Figure 5a) and ketone/alcohol functions (Figure S14). In addition, the
35 heterodimer of the two molecules investigated (limonic acid and 7OH-limonaldehyde) shows a
36 slightly less stable structure (complexation energy of -20.45 kcal/mol) than the carboxylic acid
37 homodimer (complexation energy of -22.66 kcal/mol), but is also very stable. The present
38 complexation energies obtained for acidic dimers compare fairly well with the dimerization energy of
39 -17.0 kcal/mol calculated for terpenylic acid (Claeys et al., 2009).

40 **Table 5:** Complexation energies for dimers and trimers

Complex	Oligomer type	Complexation energy	
		(raw) kcal/mol	(corrected) kcal/mol
Limononic acid dimer	Homodimer	-23.73	-22.66

7OH-limononaldehyde dimer	Homodimer	-10.09	-8.64
Limonalic acid and 7OH-limononaldehyde dimer	Heterodimer	-22.28	-20.45
Limonalic acid trimer	Homotrimer	-39.62	-35.06
7OH-limononaldehyde trimer	Homotrimer	-35.77	-31.28

1

2 Furthermore, the complexation energies of the trimers are larger than the complexation energies of
3 the dimers. So those values tend to demonstrate that the trimers are more stable than the
4 corresponding dimers. As expected again, cyclic trimers are stabilized by connecting two monomers
5 on one carboxylic function to form a large non-planar ring with three intermolecular hydrogen bonds
6 (Figure 5b). Compounds with ketone and alcohol functions present similar features (Figures S15).

7 These calculations confirm that the formation of dimers and trimers from oxygenated organic
8 compounds such as those produced in the limonene ozonolysis SOAs is possible. While investigating
9 larger-than-trimer oligomers was not possible for time-computing reasons, literature on water
10 clusters suggests that higher oligomers like tetramers and pentamers may be even more stable than
11 dimers and trimers (Miliordos & Xantheas, 2015; Temelso et al., 2011). According to the present
12 calculations and based on the structure of the products observed in the condensed phase, one can
13 conclude that various sizes of oligomers can be formed through non-covalent H-bonding during the
14 limonene oxidation by ozone (Figure S11).

15 4. Conclusion

16 In this work, the chemical composition of SOAs formed from the ozonolysis of limonene was
17 investigated through elemental analysis and high-resolution LC-QToF-MS/MS combined with DFT
18 calculations. Limited- and high-oxidation conditions were experimentally applied, showing a rapid
19 formation of particles with high O:C ratios. The further analysis of SOAs allowed the identification of
20 34 raw chemical formula related to first- and second-generation products mainly bearing carboxylic
21 acid and carbonyl functions. A huge number of oligomers up to heptamer structures were also
22 detected in both limited- and high-oxidation samples. The analysis of these oligomers indicates the
23 participation of the first- and second-generation products in the building up of these structures,
24 either through Criegee Intermediate reactions or through hydrogen bonding. The thorough analysis
25 of extracted ion chromatograms together with quantum chemical calculations on dimers and trimers
26 support the latter hypothesis that H-bonds involving carboxylic and carbonyl/hydroxyl functions play
27 a significant role in the formation of oligomers. Since non-covalent hydrogen bonding was shown to
28 be involved in α -pinene ozonolysis products (Claeys et al., 2009), other terpenes may also be
29 concerned by such oligomer-forming pathways, requiring further investigations. It is suggested that
30 these weakly-bond oligomers may serve as first clusters in particle nucleation processes, raising also
31 the question of their stability, lifetime and fate in the atmosphere. In addition, in the context of the
32 admitted relationships between the chemical composition of atmospheric particles and their health
33 impacts (Mauderly & Chow, 2008), the present work highlights the formation of large molecules
34 whose health impact mechanisms still need to be investigated. Finally, a series of linear dicarboxylic
35 acids were identified for the first time in the limonene ozonolysis products, the larger diacids also
36 participating in oligomer formation.

37 Acknowledgements

38 IMT Nord Europe acknowledges funding by the French ANR agency under contract No. ANR-11-LabX-
39 0005-01 CaPPA (Chemical and Physical Properties of the Atmosphere), the Région Hauts-de-France,
40 the Ministère de l'Enseignement Supérieur et de la Recherche (CPER Climibio and ECRIN) and the

1 European Fund for Regional Economic Development. The CLIMIBIO and ECRIN programs supported
2 by the Hauts-de-France Regional Council, the French Ministry of Higher Education and Research and
3 the European Regional Development Fund are also acknowledged. AT is grateful to the INSU-LEFE-
4 CHAT program for funding this research. FJ acknowledges Lille University for a labelled PhD grant.
5 Quantum chemistry calculations presented in this paper were carried out using the CALCULCO
6 computing platform, supported by SCoSI/ULCO (Service COmmun du Système d'Information de
7 l'Université du Littoral Côte d'Opale). IMPECS acknowledges funding by the Lille University Hospital
8 through the BonusH grant and the Institute on Environmental Sciences IRePSE (Institut de
9 Recherches Pluridisciplinaires en Sciences de l'Environnement).

10

11 **Data availability**

12 The authors will provide all the data upon request.

13

14 **References**

15 Ahmad, W., Coeur, C., Cuisset, A., Coddeville, P., & Tomas, A. (2017). Effects of scavengers of Criegee
16 intermediates and OH radicals on the formation of secondary organic aerosol in the
17 ozonolysis of limonene. *Journal of Aerosol Science*, *110*, 70- 83.

18 Atkinson, R., & Arey, J. (2003). Gas-phase tropospheric chemistry of biogenic volatile organic
19 compounds : A review. *Atmospheric Environment*, *37*(Supp. N°2), S197- S219.

20 Bach, R. D., Ayala, P. Y., & Schlegel, H. B. (1996). A Reassessment of the Bond Dissociation Energies of
21 Peroxides. An ab Initio Study. *Journal of the American Chemical Society*, *118*(50),
22 12758- 12765. <https://doi.org/10.1021/ja961838i>

23 Baltensperger, U., Dommen, J., Alfarra, M. R., Duplissy, J., Gaeggeler, K., Metzger, A., Facchini, M. C.,
24 Decesari, S., Finessi, E., Reinnig, C., Schott, M., Warnke, J., Hoffmann, T., Klatzer, B.,
25 Puxbaum, H., Geiser, M., Savi, M., Lang, D., Kalberer, M., & Geiser, T. (2008). Combined
26 determination of the chemical composition and of health effects of secondary organic
27 aerosols : The POLYSOA project. *Journal of Aerosol Medicine and Pulmonary Drug Delivery*,
28 *21*(1), 145- 154. <https://doi.org/10.1089/jamp.2007.0655>

29 Baltensperger, U., Kalberer, M., Dommen, J., Paulsen, D., Alfarra, M. R., Coe, H., Fisseha, R., Gascho,
30 A., Gysel, M., Nyeki, S., Sax, M., Steinbacher, M., Prévot, A. S. H., Sjögren, S., Weingartner, E.,

1 & Zenobi, R. (2005). Secondary organic aerosols from anthropogenic and biogenic precursors.
2 *Faraday Discussions*, 130(14), Article 14.

3 Bateman, A. P., Nizkorodov, S. A., Laskin, J., & Laskin, A. (2009). Time-resolved molecular
4 characterization of limonene/ozone aerosol using high-resolution electrospray ionization
5 mass spectrometry. *Physical Chemistry Chemical Physics*, 11, 7931- 7942.

6 Bateman, A. P., Walser, M. L., Desyaterik, Y., Laskin, J., Laskin, A., & Nizkorodov, S. A. (2008). The
7 effect of solvent on the analysis of secondary organic aerosol using electrospray ionization
8 mass spectrometry. *Environmental Science & Technology*, 42(19), 7341- 7346.
9 <https://doi.org/10.1021/es801226w>

10 Becke, A. D. (1993). Density-functional thermochemistry. III. The role of exact exchange. *The Journal*
11 *of Chemical Physics*, 98(7), 5648- 5652.

12 Boys, S. F., & Bernardi, F. (1970). The calculation of small molecular interactions by the differences of
13 separate total energies. Some procedures with reduced errors. *Molecular Physics*, 19(4),
14 553- 566.

15 Braure, T., Bedjanian, Y., Romanias, M. N., Morin, J., Riffault, V., Tomas, A., & Coddeville, P. (2014).
16 Experimental study of the reactions of limonene with OH and OD radicals : Kinetics and
17 products. *Journal of Physical Chemistry A*, 118, 9482- 9490.

18 Claeys, M., Iinuma, Y., Szmigielski, R., Surratt, J. D., Blockhuis, F., Van Alsenoy, C., Böge, O., Sierau, B.,
19 Gomez-Gonzalez, Y., Vermeylen, R., Van der Veken, P., Shagholi, M., Chan, A. W. H.,
20 Herrmann, H., Seinfeld, J. H., & Maenhaut, W. (2009). Terpenylic acid and related compounds
21 from the oxidation of α -pinene : Implications for new particle formation and growth above
22 forests. *Environmental Science and Technology*, 43(18), Article 18.

23 Clará, R. A., Marigliano, A. C. G., & Sólamo, H. N. (2009). Density, viscosity, and refractive index in the
24 range (283.15 to 353.15) K and vapor pressure of α -pinene, d-limonene, (\pm)-linalool, and
25 citral over the pressure range 1.0 kPa atmospheric pressure. *Journal of Chemical &*
26 *Engineering Data*, 54(3), 1087- 1090.

1 Clausen, P. A., Wilkins, C. K., Wolkoff, P., & Nielsen, G. D. (2001). Chemical and biological evaluation
2 of a reaction mixture of R-(+)-limonene/ozone : Formation of strong airway irritants.
3 *Environment International*, 26(7), 511- 522.

4 Crippa, M., Canonaco, F., Lanz, V. A., Äijälä, M., Allan, J. D., Carbone, S., Capes, G., Ceburnis, D.,
5 Dall'Osto, M., Day, D. A., DeCarlo, P. F., Ehn, M., Eriksson, A., Freney, E., Hildebrandt Ruiz, L.,
6 Hillamo, R., Jimenez, J. L., Junninen, H., Kiendler-Scharr, A., ... Prévôt, A. S. H. (2014). Organic
7 aerosol components derived from 25 AMS data sets across Europe using a consistent ME-2
8 based source apportionment approach. *Atmospheric Chemistry and Physics*, 14(12),
9 6159- 6176. <https://doi.org/10.5194/acp-14-6159-2014>

10 Csankó, K. (2015). *Stereoselective synthesis and self-assembling capabilities of heterocyclic cinnamic*
11 *acids* [PhD thesis]. University of Szeged.

12 Duncianu, M., Olariu, R. I., Visez, N., Riffault, V., Tomas, A., & Coddeville, P. (2012). Development of a
13 new flow reactor for kinetic studies. Application to the ozonolysis of a series of alkenes.
14 *Journal of Physical Chemistry A*, 116, 6169- 6179.

15 Dunning, T. H. (1989). Gaussian basis sets for use in correlated molecular calculations. I. The atoms
16 boron through neon and hydrogen. *The Journal of Chemical Physics*, 90(2), 1007- 1023.

17 Frisch, M. J., Trucks, G. W., Schlegel, H. B., Scuseria, G. E., Robb, M. A., Cheeseman, J. R., Scalmani, G.,
18 Barone, V., Petersson, G. A., Nakatsuji, H., Li, X., Caricato, M., Marenich, A. V., Bloino, J.,
19 Janesko, B. G., Gomperts, R., Mennucci, B., Hratchian, H. P., Ortiz, J. V., ... Fox, D. J. (2019).
20 *Gaussian 16 Rev. C.01*.

21 Gao, S., Keywood, M., Ng, N. L., Surratt, J., Varutbangkul, V., Bahreini, R., Flagan, R. C., & Seinfeld, J.
22 H. (2004). Low-Molecular-Weight and Oligomeric Components in Secondary Organic Aerosol
23 from the Ozonolysis of Cycloalkenes and α -Pinene. *The Journal of Physical Chemistry A*,
24 108(46), 10147- 10164. <https://doi.org/10.1021/jp047466e>

1 Gong, Y., Chen, Z., & Li, H. (2018). The oxidation regime and SOA composition in limonene
2 ozonolysis : Roles of different double bonds, radicals, and water. *Atmospheric Chemistry and*
3 *Physics*, 18(20), 15105- 15123.

4 Goubet, M., Soulard, P., Pirali, O., Asselin, P., Réal, F., Gruet, S., Huet, T. R., Roy, P., & Georges, R.
5 (2015). Standard free energy of the equilibrium between the trans-monomer and the cyclic-
6 dimer of acetic acid in the gas phase from infrared spectroscopy. *Physical Chemistry Chemical*
7 *Physics*, 17(11), 7477- 7488.

8 Grimme, S., Antony, J., Ehrlich, S., & Krieg, H. (2010). A consistent and accurate ab initio
9 parametrization of density functional dispersion correction (DFT-D) for the 94 elements H-Pu.
10 *The Journal of Chemical Physics*, 132(15), 154104.

11 Grimme, S., Ehrlich, S., & Goerigk, L. (2011). Effect of the damping function in dispersion corrected
12 density functional theory. *Journal of Computational Chemistry*, 32(7), 1456- 1465.

13 Grosjean, D., Williams, E. L., II, Grosjean, E., Andino, J. M., & Seinfeld, J. H. (1993). Atmospheric
14 oxidation of biogenic hydrocarbons : Reaction of ozone with b-pinene, d-limonene and trans-
15 caryophyllene. *Environmental Science and Technology*, 27, 2754- 2758.

16 Guenther, A. B., Jiang, X., Heald, C. L., Sakulyanontvittaya, T., Duhl, T., Emmons, L. K., & Wang, X.
17 (2012). The Model of Emissions of Gases and Aerosols from Nature version 2.1 (MEGAN2.1) :
18 An extended and updated framework for modeling biogenic emissions. *Geoscientific Model*
19 *Development*, 5, 1471- 1492.

20 Hallquist, M., Wenger, J., Baltensperger, U., Rudich, Y., Simpson, D., Claeys, M., Dommen, J.,
21 Donahue, N. M., George, C., Goldstein, A. H., Hamilton, J. F., Herrmann, H., Hoffmann, T.,
22 Iinuma, Y., Jang, M., Jenkin, M. E., Jimenez, J. L., Kiendler-Scharr, A., Maenhaut, W., ... Wildt,
23 J. (2009). The formation, properties and impact of secondary organic aerosol : Current and
24 emerging issues. *Atmospheric Chemistry and Physics*, 9, 5155- 5236.

1 Hammes, J., Lutz, A., Mentel, T., Faxon, C., & Hallquist, M. (2019). Carboxylic acids from limonene
2 oxidation by ozone and hydroxyl radicals : Insights into mechanisms derived using a
3 FIGAERO-CIMS. *Atmospheric Chemistry and Physics*, 19(20), 13037- 13052.

4 Heaton, K. J., Dreyfus, M. A., Wang, S., & Johnston, M. V. (2007). Oligomers in the early stage of
5 biogenic secondary organic aerosol formation and growth. *Environmental Science and
6 Technology*, 41(17), Article 17.

7 Herrmann, F., Winterhalter, R., Moortgat, G. K., & Williams, J. (2010). Hydroxyl radical (OH) yields
8 from the ozonolysis of both double bonds for five monoterpenes. *Atmospheric Environment*,
9 44(28), 3458- 3464.

10 Hoffmann, T., Bandur, R., Marggraf, U., & Linscheid, M. (1998). Molecular composition of organic
11 aerosols formed in the α -pinene/O₃ reaction : Implications for new particle formation
12 processes. *Journal of Geophysical Research*, 103(D19), Article D19.

13 Jaoui, M., Corse, E., Kleindienst, T. E., Offenberg, J. H., Lewandowski, M., & Edney, E. O. (2006).
14 Analysis of secondary organic aerosol compounds from the photooxidation of d-limonene in
15 the presence of NO_x and their detection in ambient PM_{2.5}. *Environmental Science &
16 Technology*, 40(12), 3819- 3828.

17 Johnson, D., & Marston, G. (2008). The gas-phase ozonolysis of unsaturated volatile organic
18 compounds in the troposphere. *Chemical Society Reviews*, 37, 699- 716.

19 Jokinen, T., Sipilä, M., Richters, S., Kerminen, V.-M., Paasonen, P., Stratmann, F., Worsnop, D. R.,
20 Kulmala, M., Ehn, M., Herrmann, H., & Berndt, T. (2014). Rapid autoxidation forms highly
21 oxidized RO₂ radicals in the atmosphere. *Angewandte Chemie International Edition*, 53,
22 14596- 14600.

23 Kalberer, M., Paulsen, D., Sax, M., Steinbacher, M., Dommen, J., Prévot, A. S. H., Fisseha, R.,
24 Weingartner, E., Frankevich, V., Zenobi, R., & Baltensperger, U. (2004). Identification of
25 polymers as major components of atmospheric organic aerosols. *Science*, 303(12 March),
26 Article 12 March.

1 Kendall, R. A., Dunning, T. H., & Harrison, R. J. (1992). Electron affinities of the first-row atoms
2 revisited. Systematic basis sets and wave functions. *The Journal of Chemical Physics*, *96*(9),
3 6796- 6806.

4 Kestner, N. R., & Combariza, J. E. (1999). Basis Set Superposition Errors : Theory and Practice. In
5 *Reviews in Computational Chemistry* (p. 99- 132). John Wiley & Sons, Ltd.

6 Kourtchev, I., Godoi, R. H. M., Connors, S., Levine, J. G., Archibald, A. T., Godoi, A. F. L., Paralovo, S. L.,
7 Barbosa, C. G. G., Souza, R. A. F., Manzi, A. O., Seco, R., Sjostedt, S., Park, J.-H., Guenther, A.,
8 Kim, S., Smith, J., Martin, S. T., & Kalberer, M. (2016). Molecular composition of organic
9 aerosols in central Amazonia : An ultra-high-resolution mass spectrometry study.
10 *Atmospheric Chemistry and Physics*, *16*(18), 11899- 11913. [https://doi.org/10.5194/acp-16-](https://doi.org/10.5194/acp-16-11899-2016)
11 [11899-2016](https://doi.org/10.5194/acp-16-11899-2016)

12 Krapf, M., El Haddad, I., Bruns, E. A., Molteni, U., Daellenbach, K. R., Prévôt, A. S. H., Baltensperger,
13 U., & Dommen, J. (2016). Labile Peroxides in Secondary Organic Aerosol. *Chem*, *1*(4),
14 603- 616. <https://doi.org/10.1016/j.chempr.2016.09.007>

15 Kundu, S., Fisseha, R., Putman, A. L., Rahn, T. A., & Mazzoleni, L. R. (2012). High molecular weight
16 SOA formation during limonene ozonolysis : Insights from ultrahigh-resolution FT-ICR mass
17 spectrometry characterization. *Atmospheric Chemistry and Physics*, *12*, 5523- 5536.

18 Lee, C., Yang, W., & Parr, R. G. (1988). Development of the Colle-Salvetti correlation-energy formula
19 into a functional of the electron density. *Physical Review B*, *37*(2), 785- 789.

20 Leungsakul, S., Jaoui, M., & Kamens, R. M. (2005). Kinetic mechanism for predicting secondary
21 organic aerosol formation from the reaction of d-limonene with ozone. *Environmental*
22 *Science and Technology*, *39*(24), Article 24.

23 Lin, M., Horowitz, L. W., Payton, R., Fiore, A. M., & Tonnesen, G. (2017). US surface ozone trends and
24 extremes from 1980 to 2014 : Quantifying the roles of rising Asian emissions, domestic
25 controls, wildfires, and climate. *Atmospheric Chemistry and Physics*, *17*(4), 2943- 2970.

- 1 Mauderly, J. L., & Chow, J. C. (2008). Health effects of organic aerosols. *Inhalation Toxicology*, 20(3),
2 257- 288.
- 3 Meng, L., Coeur, C., Fayad, L., Houzel, N., Genevray, P., Bouzidi, H., Tomas, A., & Chen, W. (2020).
4 Secondary organic aerosol formation from the gas-phase reaction of guaiacol (2-
5 methoxyphenol) with NO₃ radicals. *Atmospheric Environment*, 240, 117740.
- 6 Miliordos, E., & Xantheas, S. S. (2015). An accurate and efficient computational protocol for obtaining
7 the complete basis set limits of the binding energies of water clusters at the MP2 and
8 CCSD(T) levels of theory : Application to (H₂O)_m, m = 2-6, 8, 11, 16, and 17. *The Journal of*
9 *Chemical Physics*, 142(23), 234303. <https://doi.org/10.1063/1.4922262>
- 10 Morawska, L., He, C., Johnson, G., Guo, H., Uhde, E., & Ayoko, G. (2009). Ultrafine particles in indoor
11 air of a school : Possible role of secondary organic aerosols. *Environmental Science and*
12 *Technology*, 43(24), Article 24.
- 13 Ofner, J., Krüger, H.-U., Grothe, H., Schmitt-Kopplin, P., Whitmore, K., & Zetzsch, C. (2011). Physico-
14 chemical characterization of SOA derived from catechol and guaiacol – a model substance for
15 the aromatic fraction of atmospheric HULIS. *Atmospheric Chemistry and Physics*, 11, 1- 15.
- 16 Pan, X., Underwood, J. S., Xing, J.-H., Mang, S. A., & Nizkorodov, S. A. (2009). Photodegradation of
17 secondary organic aerosol generated from limonene oxidation by ozone studied with
18 chemical ionization mass spectrometry. *Atmospheric Chemistry and Physics*, 9(12),
19 3851- 3865.
- 20 Poulain, L., Fahlbusch, B., Spindler, G., Müller, K., van Pinxteren, D., Wu, Z., Iinuma, Y., Birmili, W.,
21 Wiedensohler, A., & Herrmann, H. (2021). Source apportionment and impact of long-range
22 transport on carbonaceous aerosol particles in central Germany during HCCT-2010.
23 *Atmospheric Chemistry and Physics*, 21(5), 3667- 3684. [https://doi.org/10.5194/acp-21-](https://doi.org/10.5194/acp-21-3667-2021)
24 3667-2021

1 Rohr, A. C., Wilkins, C. K., Clausen, P. A., Hammer, M., Nielsen, G. D., Wolkoff, P., & Spengler, J. D.
2 (2002). Upper airway and pulmonary effects of oxidation products of (+)- α -pinene, d-
3 limonene, and isoprene in BALB/c mice. *Inhalation Toxicology*, *14*(7), 663- 684.

4 Rosales, C. M. F., Jiang, J., Lahib, A., Bottorff, B. P., Reidy, E. K., Kumar, V., Tasoglou, A., Huber, H.,
5 Dusanter, S., Tomas, A., Boor, B. E., & Stevens, P. S. (2022). Chemistry and human exposure
6 implications of secondary organic aerosol production from indoor terpene ozonolysis.
7 *Science Advances*, *8*(8), eabj9156.

8 Saathoff, H., Naumann, K.-H., Möhler, O., Jonsson, A. M., Hallquist, M., Kiendler-Scharr, A., Mentel, T.
9 F., Tillmann, R., & Schurath, U. (2009). Temperature dependence of yields of secondary
10 organic aerosols from the ozonolysis of α -pinene and limonene. *Atmospheric Chemistry and*
11 *Physics*, *9*, 1551- 1577.

12 Shu, Y., & Atkinson, R. (1994). Rate constants for the gas-phase reactions of O₃ with a series of
13 Terpenes and OH radical formation from the O₃ reactions with Sesquiterpenes at 296 \pm 2 K.
14 *International Journal of Chemical Kinetics*, *26*(12), Article 12.

15 Simon, S., Duran, M., & Dannenberg, J. J. (1996). How does basis set superposition error change the
16 potential surfaces for hydrogen-bonded dimers? *The Journal of Chemical Physics*, *105*(24),
17 11024- 11031.

18 Stephens, P. J., Devlin, F. J., Chabalowski, C. F., & Frisch, M. J. (1994). Ab Initio calculation of
19 vibrational absorption and circular dichroism spectra using density functional force fields.
20 *The Journal of Physical Chemistry*, *98*(45), 11623- 11627.

21 Temelso, B., Archer, K. A., & Shields, G. C. (2011). Benchmark structures and binding energies of small
22 water clusters with anharmonicity corrections. *The Journal of Physical Chemistry A*, *115*(43),
23 12034- 12046. <https://doi.org/10.1021/jp2069489>

24 Tolocka, M., Jang, M., Ginter, J. M., Cox, F. J., Kamens, R. M., & Johnston, M. V. (2004). Formation of
25 oligomers in secondary organic aerosol. *Environmental Science and Technology*, *38*(5), Article
26 5.

1 Varutbangkul, V., Brechtel, F. J., Bahreini, R., Ng, N. L., Keywood, M. D., Kroll, J. H., Flagan, R. C.,
2 Seinfeld, J. H., Lee, A., & Goldstein, A. H. (2006). Hygroscopicity of secondary organic aerosols
3 formed by oxidation of cycloalkenes, monoterpenes, sesquiterpenes, and related
4 compounds. *Atmospheric Chemistry and Physics*, 6(9), 2367- 2388.
5 <https://doi.org/10.5194/acp-6-2367-2006>

6 Vosko, S. H., Wilk, L., & Nusair, M. (1980). Accurate spin-dependent electron liquid correlation
7 energies for local spin density calculations : A critical analysis. *Canadian Journal of Physics*,
8 58(8), 1200- 1211.

9 Walser, M. L., Desyaterik, Y., Laskin, J., Laskin, A., & A. Nizkorodov, S. (2008). High-resolution mass
10 spectrometric analysis of secondary organic aerosol produced by ozonation of limonene.
11 *Physical Chemistry Chemical Physics*, 10(7), Article 7.

12 Wang, L., & Wang, L. (2021). The oxidation mechanism of gas-phase ozonolysis of limonene in the
13 atmosphere. *Physical Chemistry Chemical Physics*, 23(15), 9294- 9303.

14 Waring, M. S., Wells, J. R., & Siegel, J. A. (2011). Secondary organic aerosol formation from ozone
15 reactions with single terpenoids and terpenoid mixtures. *Atmospheric Environment*, 45(25),
16 4235- 4242.

17 Warscheid, B., & Hoffmann, T. (2002). Direct analysis of highly oxidised organic aerosol constituents
18 by on-line ion trap mass spectrometry in the negative-ion mode. *Rapid Communications in*
19 *Mass Spectrometry*, 16(6), 496- 504.

20 Witkowski, B., & Gierczak, T. (2017). Characterization of the limonene oxidation products with liquid
21 chromatography coupled to the tandem mass spectrometry. *Atmospheric Environment*, 154,
22 297- 307.

23 Yang, S., Duan, F., Ma, Y., Li, H., Wang, J., Du, Z., Xu, Y., Zhang, T., Zhu, L., Huang, T., Kimoto, T.,
24 Zhang, L., & He, K. (2020). Characteristics and seasonal variations of high-molecular-weight
25 oligomers in urban haze aerosols. *Science of The Total Environment*, 746, 141209.
26 <https://doi.org/10.1016/j.scitotenv.2020.141209>

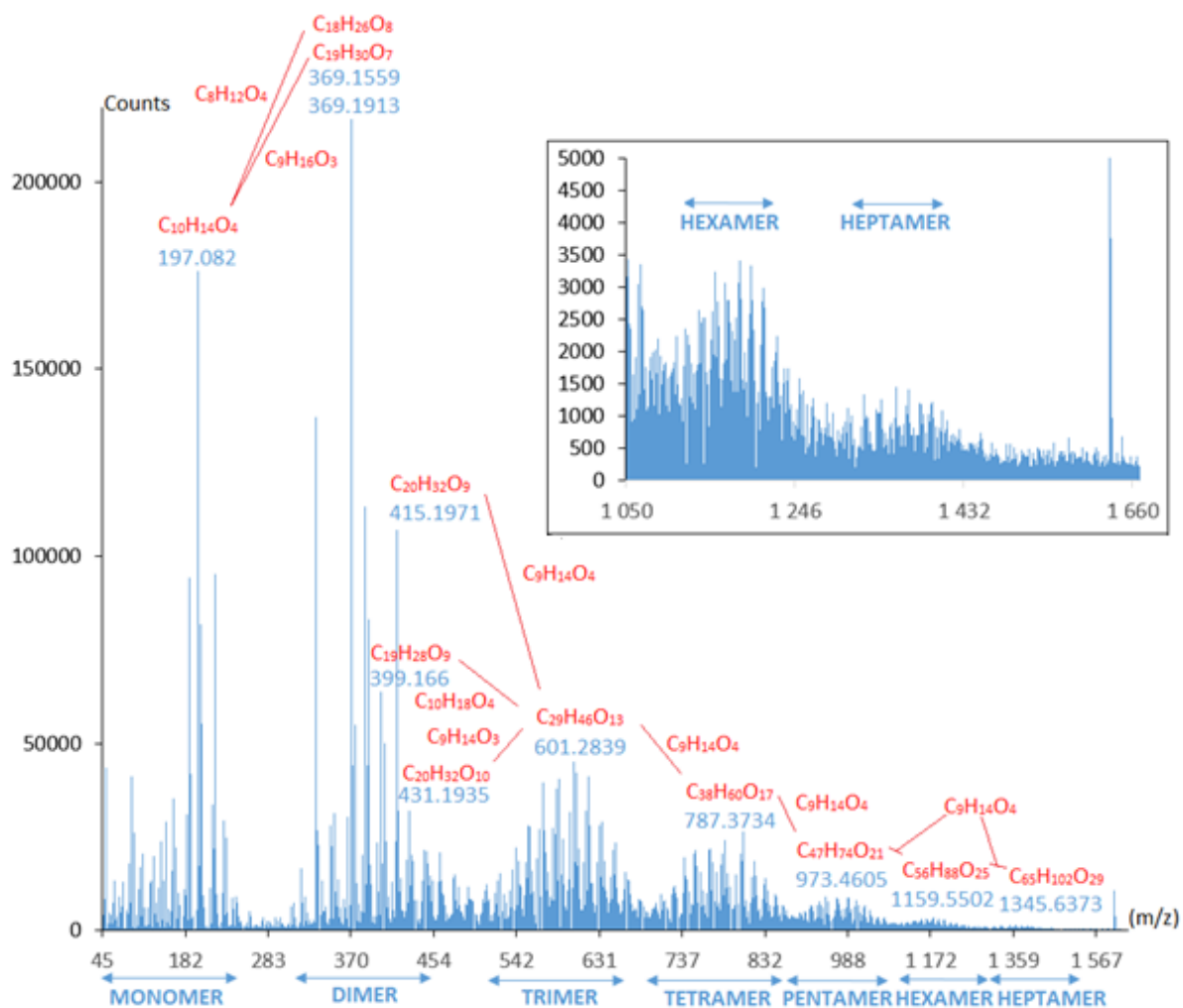
1 Yasmeeen, F., Vermeylen, R., Szmigielski, R., Iinuma, Y., Böge, O., Herrmann, H., Maenhaut, W., &
2 Claeys, M. (2010). Terpenylic acid and related compounds : Precursors for dimers in
3 secondary organic aerosol from the ozonolysis of α - and β -pinene. *Atmospheric Chemistry*
4 *and Physics*, 10, 9383- 9392.

5

6

- 1 **Figure 1:** Mass spectrum taken at a retention time of 11 min 8 s illustrating the presence of oligomers
2 up to heptamers (limited-oxidation condition). Transitions between oligomer areas are shown. All
3 the transitions correspond to exact masses of first- and second-generation products.
- 4 **Figure 2:** Mass spectrum taken at a retention time of 11 min 5 s illustrating the intra-mode
5 transitions in the dimer area. The majority of the transitions correspond to a gain or a loss of CH_2
6 (transitions $m/z = 14$) and O (transitions $m/z = 16$).
- 7 **Figure 3:** Extracted Ion Chromatograms (EIC) for $\text{C}_9\text{H}_{14}\text{O}_4$ monomer (blue line, $m/z = 185.0844$), its
8 corresponding homodimer $\text{C}_{18}\text{H}_{28}\text{O}_8$ (red line, $m/z = 371.1711$) and homotrimer $\text{C}_{27}\text{H}_{42}\text{O}_{12}$ (black line,
9 $m/z = 557.2604$). Please note that the y-axis is cut for a better view of the lower part.
- 10 **Figure 4:** EIC for a) succinic acid ($[\text{C}_4\text{H}_6\text{O}_4]^-$) = 117.0193 m/z (left) and b) pimelic acid ($[\text{C}_7\text{H}_{12}\text{O}_4]^-$) =
11 159.0663 m/z (right).
- 12 **Figure 5:** Optimized geometries with the B3LYP functional, GD3BJ dispersion correction and aug-cc-
13 pVDZ basis set for limonic acid homodimer (a) and homotrimer (b) drawn with Gaussview
14 visualisation software. The intermolecular hydrogen bonds are represented by dashed bonds.
- 15
- 16

1



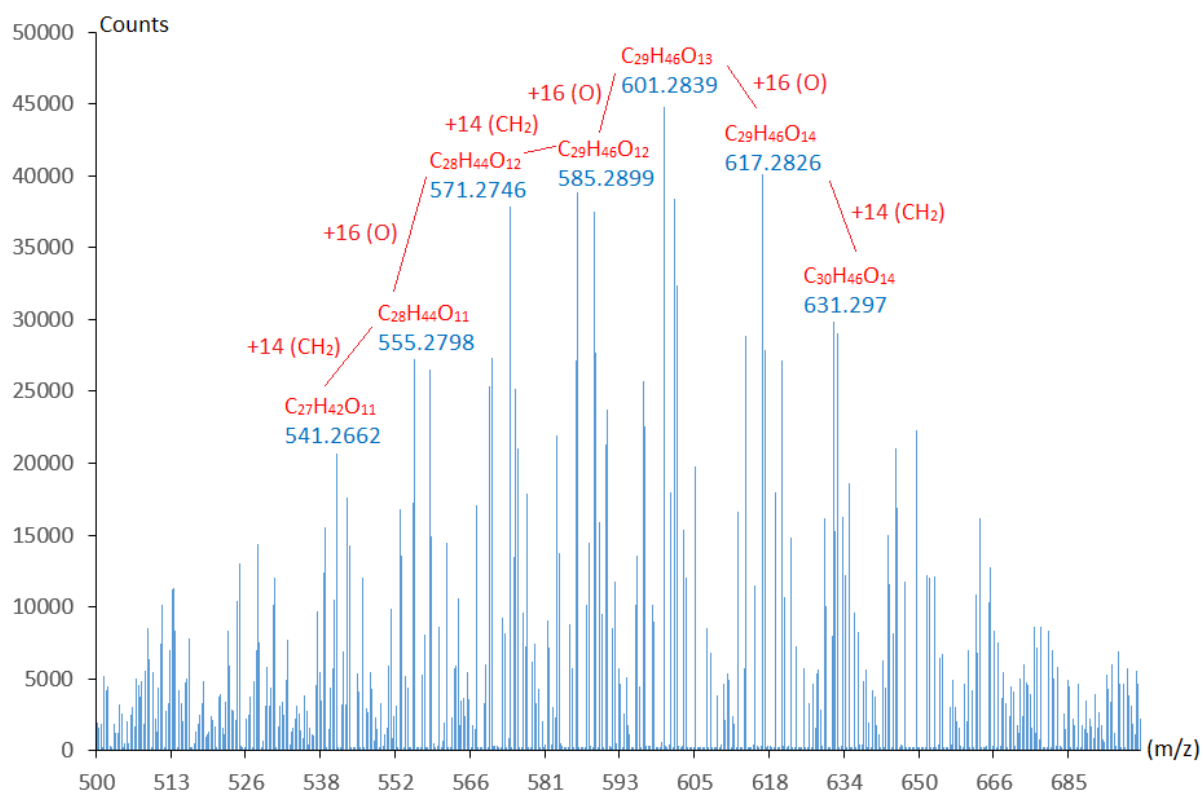
2

3

4 **Figure 1:** Mass spectrum taken at a retention time of 11 min 8 s illustrating the presence of oligomers
5 up to heptamers (limited-oxidation condition). Transitions between oligomer areas are shown. All
6 the transitions correspond to exact masses of first- and second-generation products.

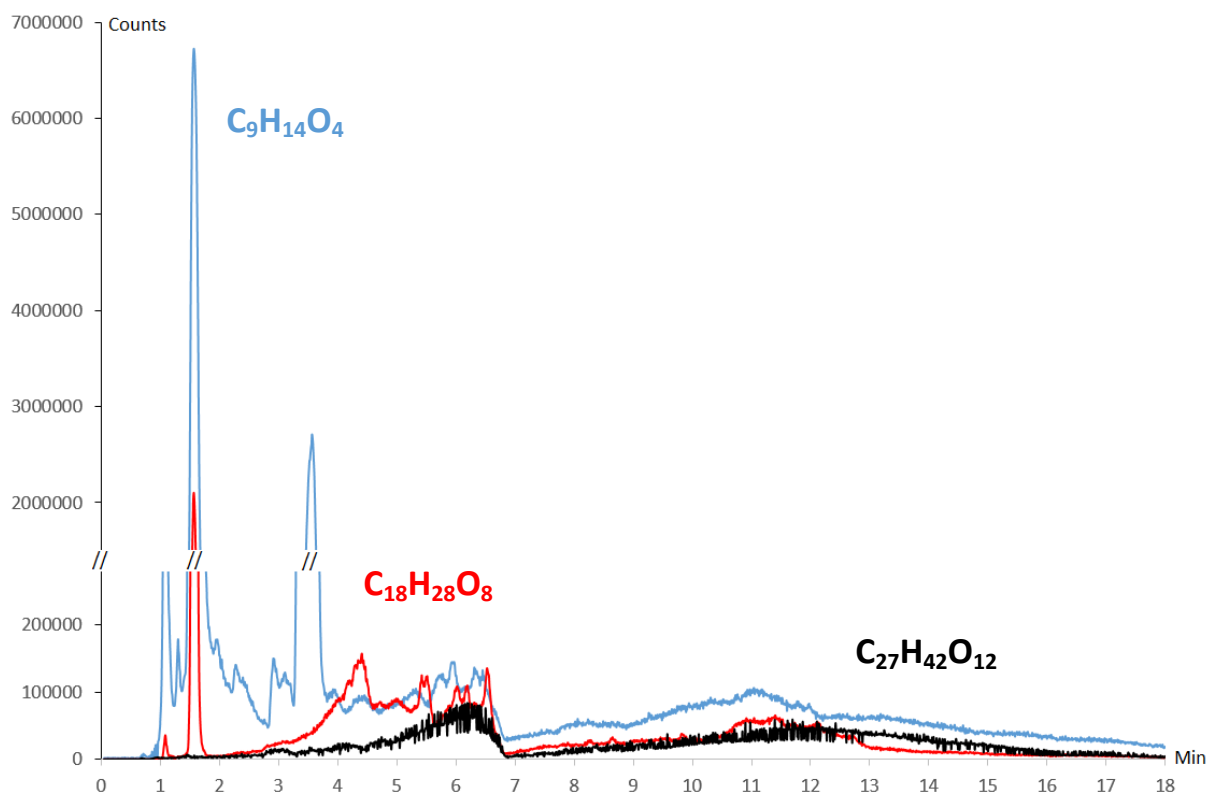
7

8



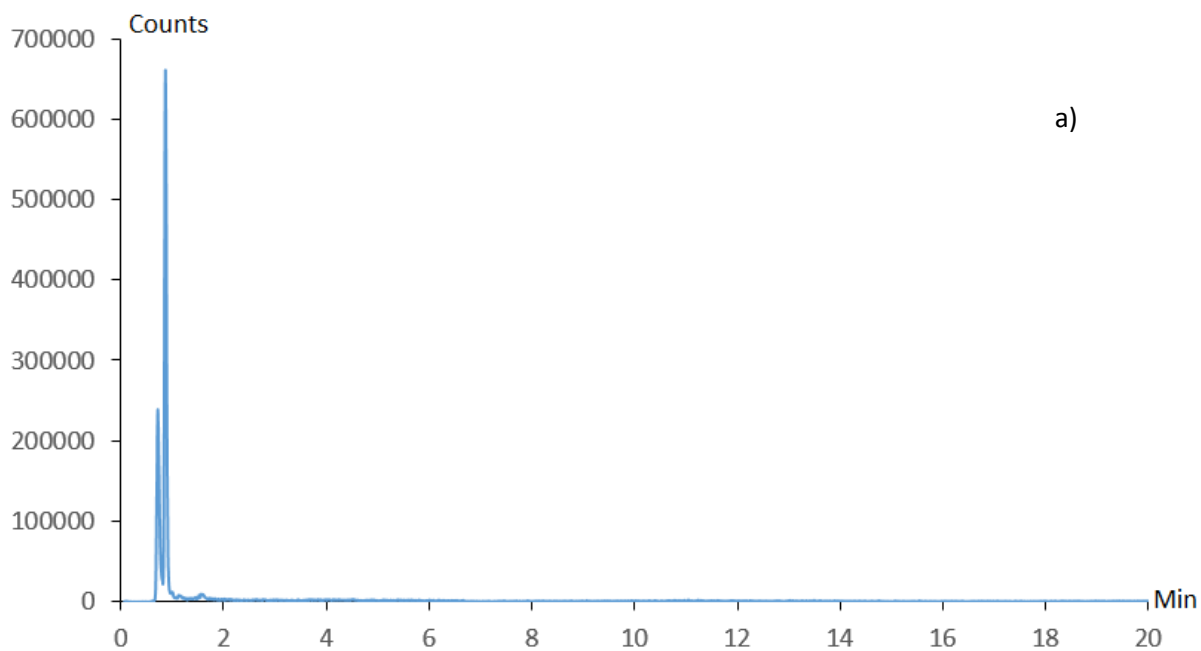
1
2
3
4
5
6
7
8

Figure 2: Mass spectrum taken at a retention time of 11 min 5 s illustrating the intra-mode transitions in the trimer area. The majority of the transitions correspond to a gain or a loss of CH₂ (transitions m/z = 14) and O (transitions m/z = 16).

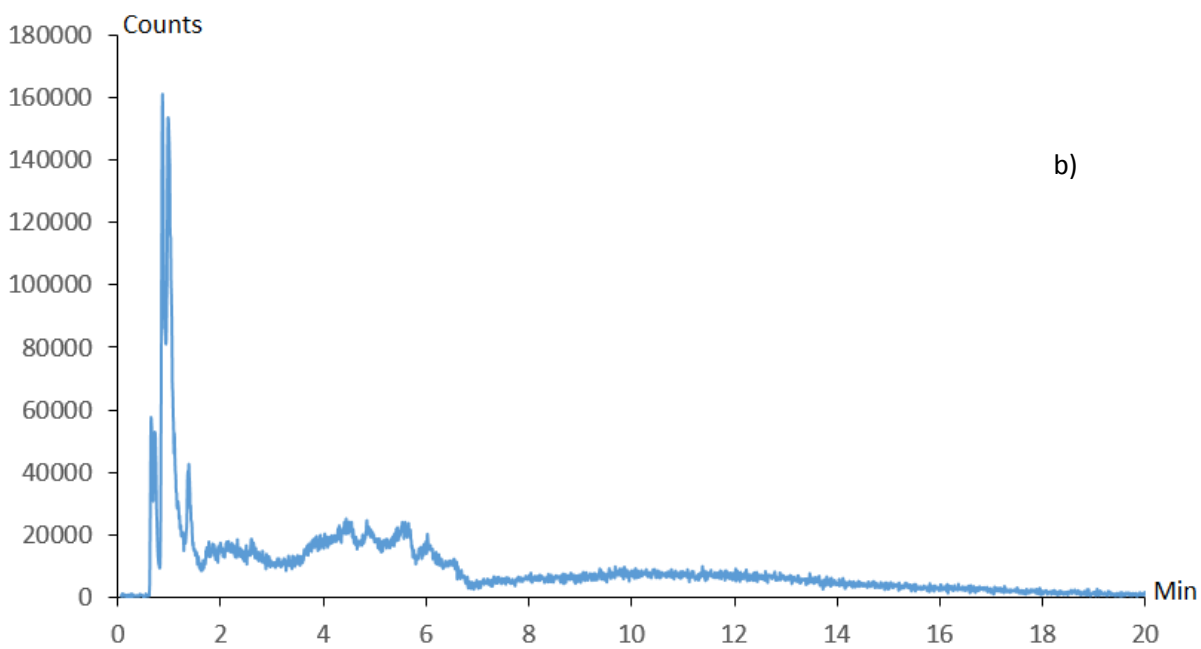


1
 2 **Figure 3:** Extracted Ion Chromatograms (EIC) for $C_9H_{14}O_4$ monomer (blue line, $m/z = 185.0844$), its
 3 corresponding homodimer $C_{18}H_{28}O_8$ (red line, $m/z = 371.1711$) and homotrimer $C_{27}H_{42}O_{12}$ (black line,
 4 $m/z = 557.2604$). Please note that the y-axis is cut for a better view of the lower part.

5



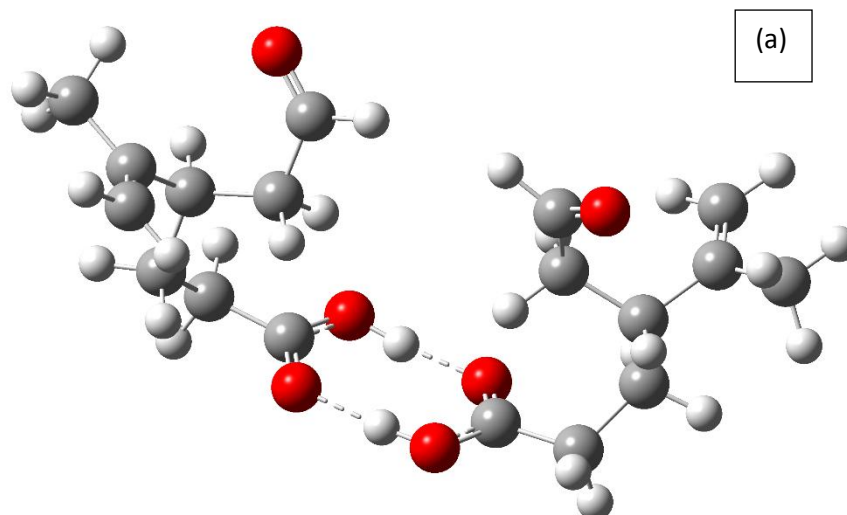
a)



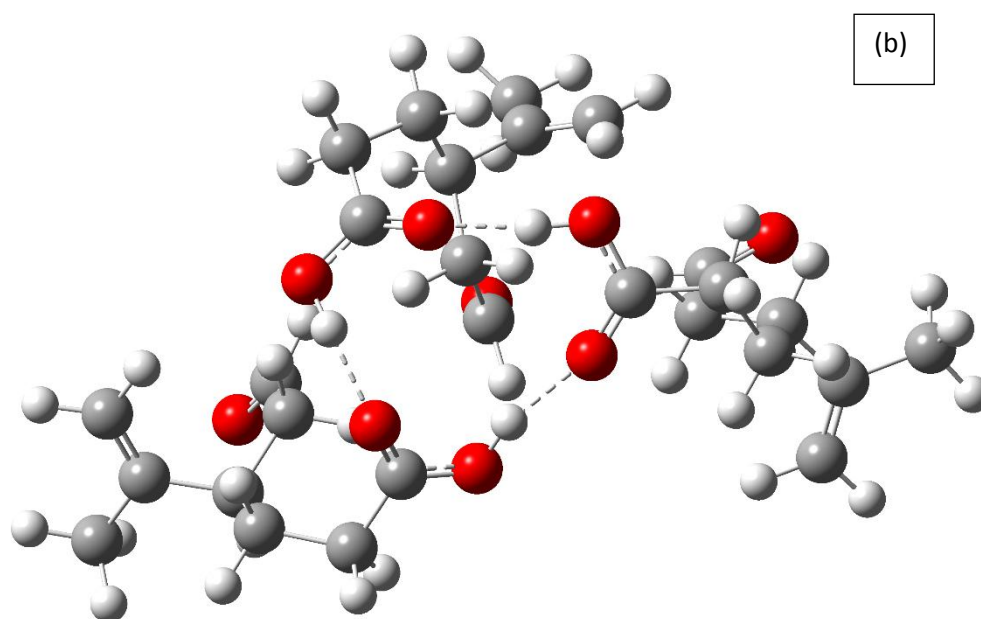
b)

1
2
3
4
5

Figure 4: EIC for a) succinic acid ($[\text{C}_4\text{H}_6\text{O}_4]^-$) = 117.0193 m/z (left) and b) pimelic acid ($[\text{C}_7\text{H}_{12}\text{O}_4]^-$) = 159.0663 m/z (right).



1
2



3
4
5
6
7

Figure 5: Optimized geometries with the B3LYP functional, GD3BJ dispersion correction and aug-cc-pVDZ basis set for limonic acid homodimer (a) and homotrimer (b) drawn with Gaussview visualisation software. The intermolecular hydrogen bonds are represented by dashed bonds.